Solar Distillation Systems: Transforming Water Scarcity Solutions in Arid Regions

[1]Rahul, [2]Dr Rashmi Dwivedi

Department of Mechanical Engineering, Sri Satya Sai University of Technology and Medical Sciences

Department of Mechanical Engineering, Sri Satya Sai University of Technology and Medical Sciences

Email-: [1]rahulcipet95@gmail.com, [2]rashmidwivedi29@gmail.com

* Corresponding Author: Rahul

Abstract: *This paper explores the evolution and optimization of solar-powered distillation systems for freshwater production, a crucial technology that has seen significant advancement since the Second World War, especially in arid regions. The study delves into the mechanics of solar stills, highlighting their capability to produce potable water through natural phenomena like evaporation and condensation. We examine the efficiency of solar stills, influenced by factors such as wind velocity, solar irradiance, and ambient temperature. The focus is on the design and efficiency of single-basin single-slope solar stills compared to innovative configurations such as double-slope solar stills. Computational Fluid Dynamics (CFD) analysis and three-dimensional CAD modeling are employed to assess the performance of these systems. The findings demonstrate that double-slope solar stills significantly outperform traditional single-slope systems in productivity, offering a promising approach to addressing global freshwater scarcity.*

Keywords: *Solar Distillation, Freshwater Production, Solar Stills, Computational Fluid Dynamics, CAD Modeling, Water Purification, Solar Energy, Distillation Efficiency, Arid Regions, Sustainable Water Solutions.*

I. INTRODUCTION

Distillation technology has been used to provide water to workers in underground factories and on ships for more than a century. Following the Second World War, there was a notable surge in the demand for freshwater in arid regions, which prompted a marked acceleration in the adoption of modern distillation methodologies. Over time, distillation costs have experienced a rapid decline, particularly in recent years, primarily attributed to the introduction of more efficient and effective equipment. Distillation is acknowledged as one among several water purification processes, with solar energy being a viable energy source for its implementation [1].

Solar energy offers the distinct advantage of cost-effective fuel utilization, although it entails certain logistical challenges, such as the need for expansive collection surfaces and the potential requirement for higher-cost equipment. In the context of utilizing solar energy for distillation, the imperative is to maintain a consistently clear water source. The progressive distillation process facilitates the selective evaporation of pure water vapor within the chamber, leading to its accumulation in the distillation unit's lid, while any impurities are effectively separated and left behind [2].

A. Working of solar still

The sun also works through natural phenomena such as evaporation and condensation, which produce rain. The configuration of solar distillation system can be concisely delineated as follows: An enclosure is outfitted with a transparent lid situated above a reservoir containing saline water. This setup harnesses solar irradiance to elevate the water's temperature, instigating the evaporation process followed by condensation on the interior surface of the optically clear, inclined lid. The resultant distilled water demonstrates a high degree of potability, characterized by its purity due to the thorough removal of all saline constituents, both inorganic and organic, along with bacterial contaminants that were originally present in the source water. Furthermore, under optimal solar exposure, the water temperature rises significantly, engendering a microbial sterilization effect by eradicating pathogenic bacteria. It is noteworthy that with time, sediment accumulation may occur at the bottom of the receptacle, necessitating periodic maintenance for its removal [3,4]. The energy prerequisite for evaporating 1 kilogram of water at an initial temperature of 30°C is approximately 2.4 x 106 joules. When subjected to a solar energy flux of 250 watts per square meter (W/m2), this energy input can yield an output of up to 9 liters per square meter per day, assuming continuous exposure over a 24-hour cycle. However, in practical application scenarios, the realized solar energy production typically falls within the range of 4-5 liters per square meter per day due to temperature fluctuations that exert an impact on the distillation process. In the contemporary context, advanced solar panels exhibit an efficiency level of approximately 30-40%. When addressing the daily drinking water requisites of human populations, which exhibit a typical range spanning from 2 to 8 liters per person, and with an average need for distilled water amounting to 5 liters per person per day, it becomes evident that a solar still system encompassing approximately 2 square meters of capacity is essential to adequately cater to the needs of each individual.

The efficiency of solar stills is subject to several influencing variables, encompassing components comprising of wind velocity, solar irradiance, ambient temperature, temperature differentia l between the glass surfaces and water, inlet water

temperature, exposed water surface area, absorber plate dimensions, water depth, and glass inclination angle. It's important to emphasize that certain factors like solar irradiance, wind velocity, and ambient temperature fall under the purview of meteorological conditions and, as such, remain beyond human control or manipulation. On the contrary, various factors like the surface area exposed to water, dimensions of the absorber plate, inlet water temperature, water depth, as well as the angle of the glass cover offer possibilities for intentional modification for the enhancement of the overall efficiency of solar stills. A thorough exploration of these influencing factors has spurred ongoing endeavors to introduce various modifications and refinements intended to augment the performance as well as productivity of solar still systems. Through meticulous analysis of these multifaceted factors, continuous efforts are focused on advancing the design and operational aspects of solar stills to achieve heightened levels of efficiency [5].

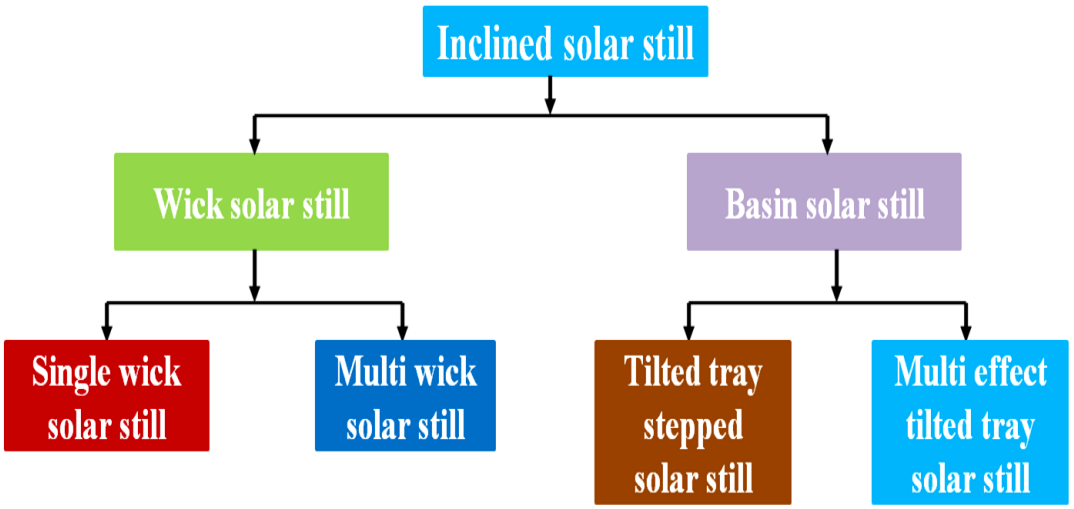

Fig. 1 Types of inclined solar still [6]

B. Working principle of solar distillation device

The operational principle of solar panels mirrors that of non-battery systems. The fundamental design of a standard solar apparatus has been illustrated by figure 1. A standard configuration of a solar still comprises a singular tank containing brine, enclosed by a single slanted glass lid. Typical materials used in constructing the basin of a solar still are copper, aluminum, or galvanized iron (GI) sheets. The interior surface of the basin is often coated with black paint to enhance its ability to absorb solar radiation more effectively. In order to reduce the loss of heat from the basin to the external environment, insulation materials are strategically placed around the sides and the bottom of the basin. This insulation acts as a barrier, helping to retain heat within the basin, thereby improving the efficiency of the solar still in converting water to vapor. This insulation is typically achieved through the use of materials such as wood, thermocol, or glass wool. At the top of the basin, a transparent glass or plastic cover is installed. The cover of the solar still plays a crucial dual role: it not only allows maximum solar radiation to enter the basin but also retains the generated water vapor inside the still. To achieve optimal solar radiation absorption, the cover is usually angled to match the region's latitude. This alignment ensures the most effective capture of sunlight, improving the still's efficiency in vaporizing water.

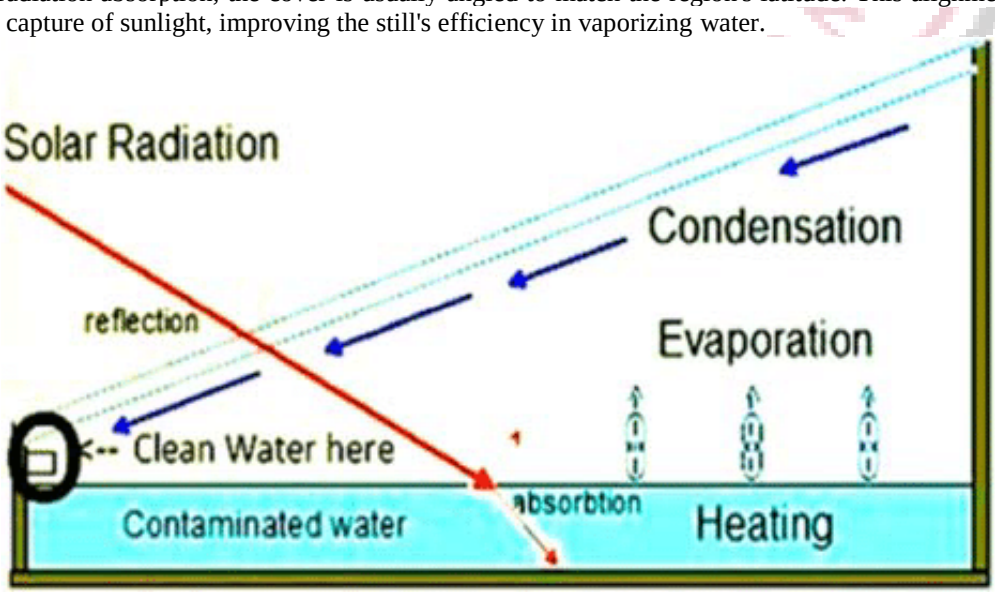

Fig. 2 Solar Radiation

Sunlight passes through the cover and gets absorbed by the basin, causing an increase in the basin's temperature. This heat is then transferred to the saline water, causing only the water component to evaporate selectively. The water vapor then rises, meeting the cooler cover, leading to its condensation on the cover's inner surface. This process produces pure condensed water, which is then gathered in a distillation trough. For enhancing this procedure, the system includes an inlet for introducing additional saline water into the basin, along with a drainage outlet at the basin's base for eliminating accumulated salts.

C. Single basin single slope solar still

While retaining its fundamental simplicity in both operation and construction, the single-basin solar plant is cost-effective and characterized by minimal maintenance requirements. Nevertheless, it is burdened by inherent limitations in terms of productivity. To address this challenge, numerous researchers have undertaken endeavors aimed at circumventing the constraints associated with a single-basin, single-slope configuration. These concerted research efforts have yielded a diverse array of innovative designs and configurations for solar stills, each offering distinct advantages over the conventional single-basin solar still.

These innovative designs encompass double-tilt solar stills, multi-basin weir-type solar stills equipped with an expanding basin structure (multi-stage or multi-basin), stepped-slope, reverse-flow and inclined solar stills. These alternative configurations have consistently demonstrated significantly enhanced yield compared to their conventional single-basin counterparts. Additionally, researchers are actively investigating methods to increase the productivity of solar stills by integrating them with other solar thermal systems. This includes combining solar stills with flat plate solar collectors, linking vacuum tube collectors with parabolic concentrators, and employing solar pond solar stills, among various strategies. In the domain of pioneering research, a variety of top cover shapes for solar stills have been investigated. These include V-shaped, spherical, triangular prism, hemispherical, pyramidal (both triangular and square), tubular, as well as conical designs. These adjustments are made with the intention of enhancing the absorption of solar energy, which in turn increases the overall effectiveness of solar stills. Of paramount importance, research outcomes have revealed that daily productivity gains in solar stills can be achieved through the incorporation of fins composed of varied wick materials on the absorber plate. This enhancement, in conjunction with the utilization of energy storage materials (both sensible and latent), proves effective even in scenarios with limited or absent solar power availability. Numerous researchers have assessed various configurations of solar stills. These studies have highlighted that different designs of solar stills yield divergent outcomes, rendering the optimization of solar still design a challenging task based solely on existing findings. Upon conducting a comprehensive review, it is suggested that, in the context of a multi-tank solar still, an optimal configuration comprises three tanks to achieve maximum yield.

II. LITERATURE REVIEW

Sivakumar, V., & Sundaram, E. G. [7] Solar desalination is a method that converts saltwater or brackish water into drinkable water by utilizing solar energy. The rising need for potable water is driven by factors such as population growth and industrialization. Solar energy serves as the primary energy source for this conversion process, facilitated by a device called a solar still. Solar stills are broadly categorized into two types: active and passive. Passive solar stills function without requiring external, high-grade energy sources such as electricity; they depend solely on naturally available solar energy to generate fresh water. On the other hand, active solar stills may use additional energy inputs to enhance their operation. The efficiency and effectiveness of both active and passive solar stills are determined by a combination of environmental factors, including various weather conditions, as well as by specific design characteristics and operational parameters unique to each type. These factors collectively influence the quantity and quality of freshwater produced by these solar stills. Meteorological factors, being governed by natural forces, remain beyond human control. Researchers have conducted comprehensive investigations involving the development of mathematical models, experimental studies, and validation processes across numerous types of solar stills. The endeavors in this field are focused on systematically fine-tuning both the design elements and operational variables to boost the performance of both active and passive solar stills. This document presents an extensive review of various strategies and techniques that have been implemented in past years to enhance the efficiency and effectiveness of these solar stills. It delves into the array of approaches adopted to optimize their functionality, covering advancements and modifications made to improve their capacity for freshwater production, energy consumption, and overall operational efficacy.

Samee, M. A., et. al. [8] In the arid regions of southern and southwestern Pakistan, the persistent issue of inadequate access to potable water is a pressing concern. The available groundwater sources in these areas are typically characterized by high salinity levels, rendering them unsuitable for direct human consumption. Pakistan's geographical location places it within a region with abundant solar insolation, offering a significant opportunity to harness solar energy for the purpose of converting saline water into potable water. Among the various available methods, solar stills emerge as the most cost-effective and practical means to achieve this objective. For tackling the unique challenges of this area, a single-basin solar

still was carefully crafted for the geographic location of 33.3° North latitude. Extensive computations were executed to ascertain the most advantageous angle for the glass cover in a solar still, identifying 33.3 degrees as the ideal angle for both summer and winter use. During an eight-day trial in July 2004, a solar still with a 0.54 square meter basin was able to average 1.7 liters of potable water production per day. This still's efficiency was measured at 30.65%, with its highest hourly production recorded at 0.339 liters at 1:00 PM. The effectiveness of the solar still in a practical setting was further verified by using it to desalinate water from Islamabad's Simly Dam filtration plant. The initial water quality metrics, including conductivity, total dissolved solids (TDS), and pH, were recorded at 1.291 mS/cm, 370 ppm, and 6.72 respectively. Post-desalination, a significant improvement in water quality was observed, with TDS reduced to 30 ppm, conductivity to 41 µS/cm, and pH adjusted to 6.5. Groundwater from Islamabad's PIEAS colony, which initially had readings of 544 ppm, 1.668 mS/cm, and a pH of 6.78, also showed considerable improvement post-desalination, with the figures reducing to 84 ppm, 31 µS/cm, and a pH of 5.74. Furthermore, a laboratory-prepared water sample initially displayed values of 17663 ppm for TDS, 85.3 mS/cm for conductivity, and a pH of 7.58. After desalination, these parameters significantly improved to 226 ppm for TDS, 88.5 µS/cm for conductivity, and a pH of 6.13. Crucially, these results conform to the guidelines set forth by the World Health Organization (WHO) for drinking water quality, affirming the suitability of the desalinated water for human consumption.

Kabeel, A. E., & El-Agouz, S. A. [9] The single-effect solar still is a straightforward solar device employed for the transformation of accessible brackish or wastewater into drinkable water. This apparatus presents various benefits, such as simple fabrication using locally available materials, cost-efficiency, and minimal maintenance needs. Furthermore, it can be managed by individuals with limited technical knowledge. Numerous research efforts have been dedicated to improving the efficiency and output of solar stills. In-depth analysis of their operation shows that the water level in the basin is a significant factor in influencing their overall efficiency. Furthermore, the analysis has revealed that solar stills equipped with covers inclined at an angle matching the local latitude consistently receive solar radiation nearly perpendicular to their surface throughout the year. Additionally, productivity experiences improvement as cover thickness decreases and thermal conductivity increases.

The choice of material for the solar still basin plays a critical role in enhancing absorption, heat storage, and evaporation processes. Rubber has emerged as the most effective basin material for optimizing these aspects. Previous studies have also highlighted the significant enhancement in daily production achieved by employing supplementary features such as fins, stepped configurations, and sponge cubes. Integration of a solar collector, external reflector, internal condenser, hot water tank, as well as greenhouse with the solar still has proven to be an effective means of increasing productivity. Notably, the utilization of solar tracking mechanisms has been found to be superior to fixed systems in boosting solar still productivity. Furthermore, the adoption of phase change materials (PCMs) has exhibited greater effectiveness, particularly when dealing with smaller masses of basin water during the winter season.

Nayi, K. H., & Modi, K. V. [10] The provision of reliable, high-quality potable water is of paramount significance for various applications, including agricultural and industrial use, as well as for the well-being of communities. Solar desalination has become a vital technique for producing drinking water, especially in areas with warm climates or in remote regions suffering from water shortages, and where traditional electrical resources are scarce. Lately, considerable focus has been placed on developing different solar still configurations to overcome the challenges inherent in the conventional single-basin, single-slope solar stills. Among these innovative developments, the pyramid solar still has gained prominence. A comprehensive analysis of research endeavors conducted by multiple investigators in this domain has revealed that pyramid solar stills exhibit superior efficiency and cost-effectiveness in comparison to their conventional single-slope, single-basin counterparts. As such, this review paper serves as a valuable resource for researchers, providing an in-depth understanding of the fundamental principles underpinning pyramid solar stills, their relevance, evolution, and the associated challenges. Furthermore, it offers insights into strategies aimed at optimizing their thermal performance and enhancing their economic viability.

Sathyamurthy, R., et. al. [11] Water represents a critical resource vital for the sustenance of all life forms on Earth. Despite the planet's limited reserves of potable water, communities in both rural and urban settings often grapple with the consequences of consuming contaminated water, leading to the prevalence of waterborne diseases. Even groundwater, a potential source of freshwater, demands rigorous treatment before it can be considered safe for human consumption. Compounding this issue is the fact that saltwater, containing both dissolved and undissolved constituents, remains unsuitable for various domestic applications, including cleaning, washing, and bathing. The study conducts a comprehensive examination of a solar still system that integrates solar collectors. This approach has been devised for enhancing the potable fresh water production. Moreover, it is essential to acknowledge that these methods may not be

economically viable for households with limited or modest incomes. The review encompasses an evaluation of key factors such as water yield, economic considerations, and the payback period associated with various solar still configurations. To summarize, this investigation suggests potential remedies, such as the incorporation of economical solar water heaters and the application of nanofluids within these systems, to tackle the existing obstacles in ensuring access to clean water.

Panchal, H. N., & Patel, S. [12] The majority of Earth's surface is enveloped by saline water, while fresh water remains limited in availability. At the same time, the demand for potable water is consistently rising in tandem with the global population growth. In this context, solar desalination presents itself as a viable solution to address this pressing requirement. This technology harnesses solar energy to remove salts and other impurities from water, making it suitable for human consumption. As the world's population continues to expand, the need for sustainable and accessible sources of clean water becomes increasingly urgent, and solar desalination offers a promising avenue to fulfill this growing demand without exacerbating environmental concerns. It involves the transformation of contaminated water into purified water using a device known as a solar still. Numerous researchers have dedicated considerable attention to examining the factors impacting the effectiveness of solar stills and enhancing their performance. The research conducted in this field examines a variety of design elements and environmental conditions that play a significant role in determining the productivity of solar stills. These studies delve into how factors such as the structural configuration of the stills, material choices, and the incorporation of technological enhancements, along with external environmental variables like solar intensity, ambient temperature, and humidity, impact the efficiency of water distillation. By exploring these aspects, the research aims to optimize the design and operation of solar stills for maximum water production efficiency under varying environmental conditions.

Kadhum, J. A. [13] The worldwide issue of restricted access to safe drinking water stands as a critical concern, profoundly impacting the health and long-term viability of human communities globally. This challenge not only affects individual health and wellbeing but also has broader implications for the sustainable development of societies. Ensuring reliable access to clean water is essential for maintaining public health, supporting economic growth, and fostering resilient communities in diverse regions across the planet. Solar distillation systems have emerged as a potential remedy to address this pressing issue. These systems harness solar energy to facilitate the production of clean water, serving diverse applications such as laboratory processes, drinking water generation, and agricultural use. The scalability of solar distillation systems allows adaptation to specific operational requirements. This research initiative aims to elevate the productivity of solar distillation systems through innovative design modifications. Two distinct types of solar distillers have been developed and subjected to rigorous testing. The first adheres to a conventional solar tub configuration, capable of yielding a daily output of 3 liters per square meter (L/m^2) during the summer season. Conversely, the Type II solar distiller features a graduated design that optimizes solar exposure, resulting in a notable 22% increase in daily distilled water production. These advancements hold promise for addressing the pressing global need for reliable sources of clean drinking water.

III. OBJECTIVES

The primary goal of this study is to assess the maximum water output achievable from a double-slope solar still basin and evaluate its efficiency. The specific objectives of this research are as follows:

- Enhance the productivity of the solar still by experimenting with various geometric parameters.
- Compare the outcomes of the conventional solar still design with a new proposed design, analyzing variables such as temperature, mass flow rate, and efficiency optimization.
- Validate the analytical results of the new solar still design by comparing all relevant parameters with those of the conventional design.

IV. METHODOLOGY

A. Numerical analysis of solar still

The solar still is designed to be completely sealed to prevent any vapor leakage and boasts excellent insulation properties. Within the system, temperature changes are minimal, both in the Phase Change Material (PCM) and in the tank water. Heat conduction is efficient in one direction and transfers energy from the tank liner to the PCM. The presence of condensate and glass water does not prevent the flow of heat through the glass cover. In addition, the absorption properties of the water in the tank and the water used for cooling between the layers of glass are negligible. Cooling water has a low heat capacity and is assumed experience the temperature fluctuations along its path.

Phase Change Material Energy Storage

The energy stored by PCM during the day = K_{pcm}

When the temperature of PCM is not equal to mean temperature

$$K_{PCM} = \left[\frac{N_e}{A_r}\frac{dT_{pcm}}{dt}\right] = \left[\frac{l-T_{pcm}}{Tr}\right] - Q_{loss} \quad (4.1)$$

When the temperature of PCM is equal to mean temperature

$$K_{pcm} = \frac{m_{pcm}.L_{pcm}}{\mathrm{Ar}.\Delta t} = \left[\frac{\mathrm{l}-T_{pcm}}{\mathrm{Tr}}\right] - Q_{\mathrm{loss}} \quad (4.2)$$

N_e= Equivalent heat capacity of PCM

A_r = Area of basin water (m^2)

T_{pcm} = Temperature of PCM

l= Temperature of liquid

R_t = Total thermal resistance of PCM (m^2K/W)

Q_{loss} = heat loss

N_{pcm} = Latent heat of PCM (J/kg)

Equivalent heat capacity for solid PCM

$$N_e = m_{pcm}.C_{p,pcm} \ \ when\ T_{pcm} < T_m \quad (4.3)$$

Equivalent heat capacity for liquid PCM

$$N_e = m_{pcm}.C_{p,pcm} \ \ when\ T_{pcm} > T_m \quad (4.4)$$

$$T_r = \frac{1}{h} + \frac{x_p}{k_p} + \frac{x_{tube}}{k_{tube}} \quad (4.4)$$

h = Convective heat transfer coefficient, *h* to be 135 W/m2.K

x_p = Thickness of plate (m).

x_{tube} = Thickness tube respectively (m).

k_p = Thermal conductivity of plate (W/m.K)

k_{tube} = Thermal conductivity of tube (W/m.K)

Heat loss from the PCM to surrounding

$$Q_{loss} = U.\left(T_{pcm} - T_a\right) \quad (4.5)$$

$L =$ Losses coefficient

$$U = \left(\frac{t_i}{k_i} + \frac{1}{h_{lb-a}}\right) - 1 \quad (4.6)$$

P_i= Thickness of insulation

Q_i= Thermal conductivity of insulation

h_{lb-a} = External heat transfer from the surface to ambient

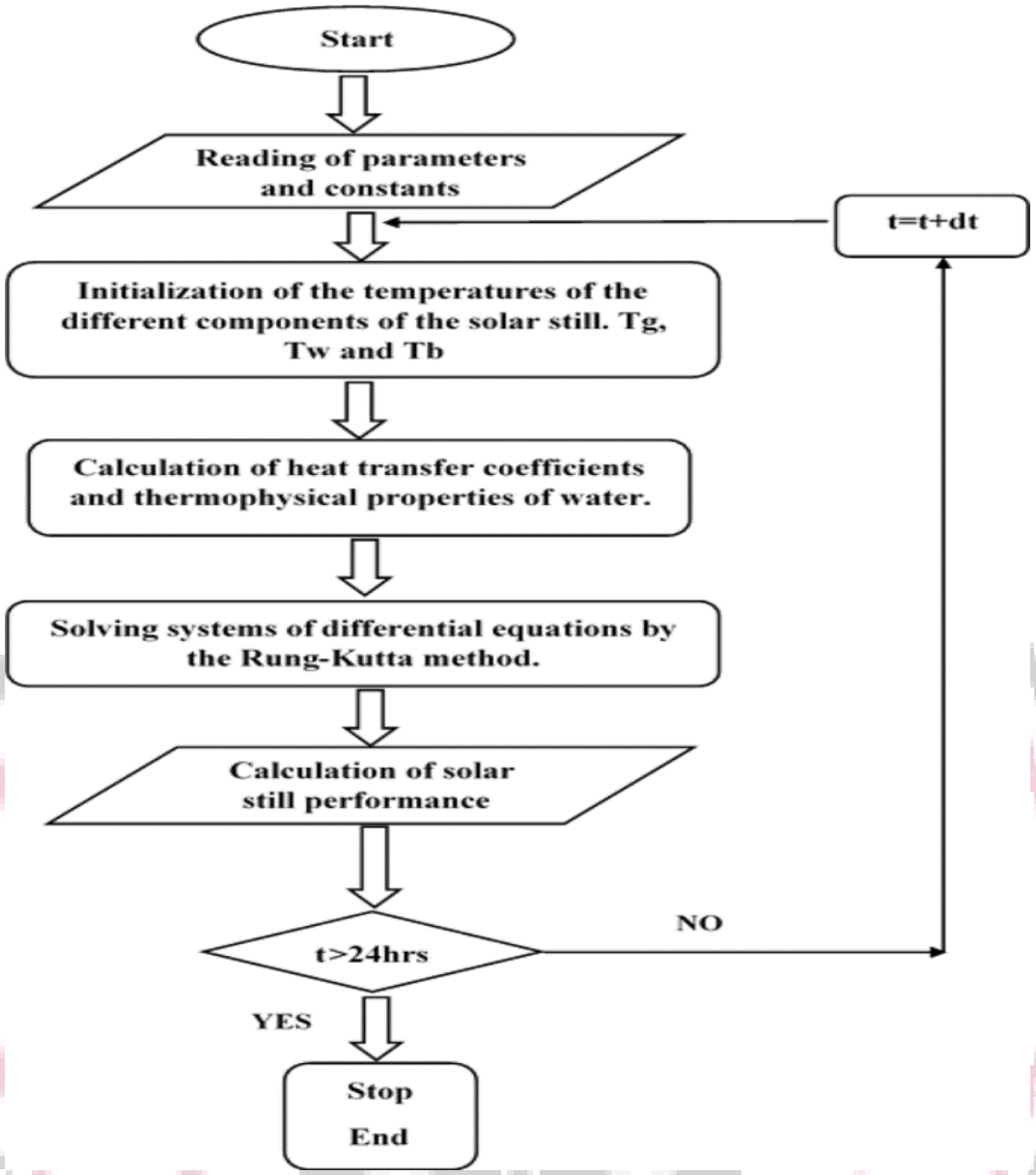

Fig. 3 Modeling Solar Still Performance with Runge-Kutta Method

Still's efficiency and productivity

To calculate the hourly productivity we use:

$$P_h = \frac{h_{evap}\,(T_w - T_g)\times 3600}{\lambda} \tag{4.7}$$

h_{evap} = Heat transfer coefficient for evaporation between the water in the basin and the glass

$$h_{evap} = 16.273 \times 10^{-3} \times h_c \times \left[\frac{P_w - P_g}{T_w - T_g}\right]$$

h_c = Convection heat transfer coefficient from the water in the basin to the glass cover

P_w = Vapour pressure of basin water

P_g= Vapour pressure of glass water

$$P = \exp\left[25.317 - \frac{5144}{T+273}\right]$$

T_w= Temperature of water

T_g= Temperature of glass

$$h_c = 0.884\left[T_w - T_g + \left\{\frac{(P_w - P_g)(T_w + 273)}{268900 - P_w}\right\}\right]^{1/3}$$

λ = Vaporization of water's Latent heat during the day (J/kg)

The daily productivityP_d and efficiency η_d are given by

$$P_d = \sum_{24\ hr} P_h \quad (4.8)$$

$$\eta_d = \frac{P_d \times \lambda_{av}}{A_p \times \sum Q_r \times \Delta t} \quad (4.9)$$

λ_{av}= average latent heat of water vaporization throughout the day

A_p= basin area

Δt = time interval of sunshine hour

Q_r = Solar irradiation received by the unit (W/m^2)

$$Q_r = 864 \exp\left[-\left(\frac{t - 13.11}{4.064}\right)^2\right]$$

Where t is the solar time in (hour),

B. CFD Analysis of Solar Still

CFD involves the study of heat transfer as well as fluid flow in systems through computer simulations. This approach is highly effective and finds application in various industrial and non-industrial sectors. In the course of our investigation, a comprehensive Computational Fluid Dynamics (CFD) analysis was executed on a solar device incorporating a phase change material. The analytical study was carried out utilizing the Ansys Fluent software, enabling a detailed examination of the fluid dynamics and thermal behavior within the system. This methodological approach provided a robust framework for understanding the complex interactions and heat transfer mechanisms associated with the integration of phase change materials in solar devices. The utilization of Ansys Fluent software facilitated a thorough exploration of the thermal dynamics, contributing to a nuanced comprehension of the performance and efficiency of the solar device under scrutiny. This computational analysis is based on fundamental equations, comprising the momentum equation, the continuity equation, and the energy equations. CFD centers around numerical algorithms equipped to solve fluid flow problems. To take advantage of the problem-solving capabilities, CFD packages typically include sophisticated user interfaces involving three primary components:

Preprocessor,

Solver a

Post-processor.

Pre-processor

The preprocessing stage entails inputting the flow problem's parameters into the CFD program using an intuitive user interface. This input is then converted into a format compatible with the solver. User activities during preprocessing encompass:

- Defining the geometry of the region under investigation, often referred to as the computational domain.
- Grid generation, which involves dividing the domain into smaller units to create a grid or network of cells or control volumes.
- Choosing the physical and chemical phenomena to simulate.
- Specification of liquid properties.
- Defining suitable boundary conditions.

Within each cell, various flow problem parameters (such as pressure, velocity, temperature, etc.) are defined at the nodes. The precision of the CFD solution can be influenced by the grid's cell count, as a greater number of cells typically leads to increased solution accuracy. Advanced software can automatically adjust the grid, particularly in areas with rapid changes. It is worth noting that considerable groundwork is still needed before these techniques can be robustly incorporated into commercial CFD software.

Solver

Numerical CFD problem solving techniques include three distinct streams: finite difference, finite element, and spectral methods. A specific finite difference formulation is used in CFD problems, exemplified by software comprising of

FLUENT, CFX/ANSYS, STAR-CD, and PHOENICS. The numerical algorithm in this step includes the following processes:

- Solving algebraic equations by the iterative method.
- Discretization involves converting the resultant integral equations into a set of algebraic equations.
- Integration of the governing fluid flow equations over all finite control volumes within the domain.

The finite volume method (FVM) is characterized by its incorporation of a control volume as its primary step, distinguishing it from other computational fluid dynamics (CFD) techniques. This fundamental component guarantees the precise preservation of pertinent properties for every discrete cell dimension within the computational area. The preservation of a common flow parameter, be it velocity or an enthalpy component, within a finite control volume is articulated through a comprehensive balance that takes into account multiple processes contributing to its augmentation or diminution.

Post-processor

The post-processing phase encompasses additional processing and visualization steps for the obtained results. In this stage, there is a need to showcase and present various aspects such as:

- Domain geometry and grid representation.
- Line and shaded contour plots.
- 2D and 3D surface rendering.
- Color PostScript output.
- Vector charts.
- Contour diagrams.

More recently, these characteristics may encompass dynamic result presentation via animations. Alongside graphical elements, all CFD software generates dependable alphanumeric output and provides options for exporting data to facilitate additional manipulation.

C. Computational fluid dynamics analysis's algorithm

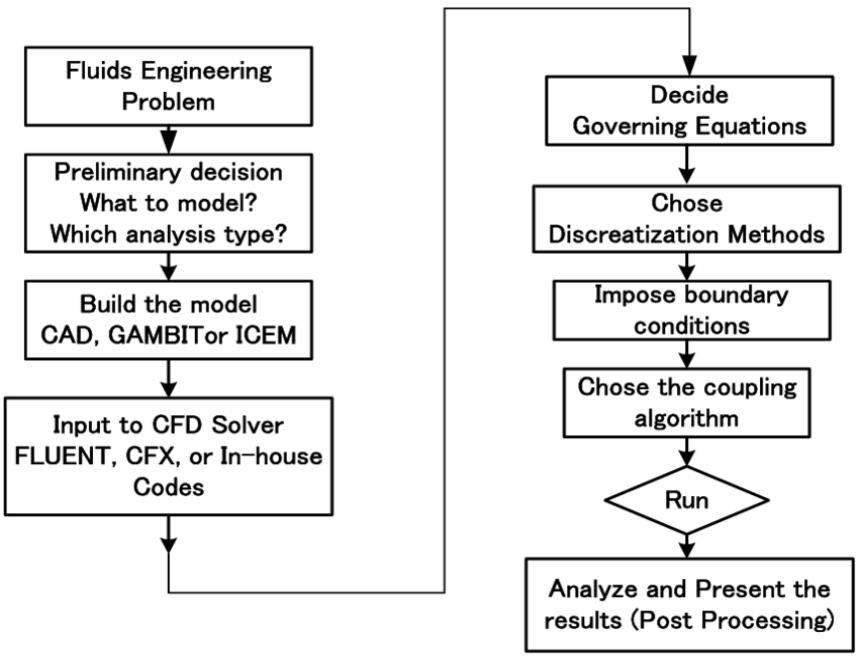

Fig. 4. Computational fluid dynamics analysis's algorithm

D. Governing Equations

The primary goal is to assess the thermal characteristics and velocity distribution resulting from the temperature gradient in a greenhouse solar dryer.

Conservation of mass or continuity equation

The expression for mass conservation, commonly referred to as the continuity equation, can be expressed in the following manner:

$$\frac{\partial \rho}{\partial t} + \nabla.(\rho\, \vec{v}) = S_m \quad (4.10)$$

In the case of 2D axisymmetric geometries, the continuity equation is expressed as follows, with

"S_m" Signifying the mass introduced into the continuous phase or any sources specified by the user:

$$\frac{\partial \rho}{\partial t} + \frac{\partial}{\partial x}(\rho v_x) + \frac{\partial}{\partial r}(\rho v_r) + \frac{\rho v_r}{r} = S_m \quad (4.11)$$

Here, the radial coordinate is represented by *r*, the axial coordinate is denoted by *x*, the axial velocity is represented by v_x, and v_r stands for the radial velocity.

Momentum Conservation Equations

The conservation of momentum in an inertial reference frame is defined as:

$$\frac{\partial}{\partial t}(\rho\vec{v}) + \nabla.(\rho\vec{v}\vec{v}) = -\nabla p + \nabla.(\bar{\bar{\tau}}) + \rho\vec{g} + \vec{F} \quad (4.12)$$

Where p= static pressure

$\rho\vec{g}$ = gravitational body force

$\bar{\bar{\tau}}$ = stress tensor, and

$\vec{F}$ = external body forces

The stress tensor $\bar{\bar{\tau}}$ is given by

$$\bar{\bar{\tau}} = \mu\left[(\nabla\vec{v} + \nabla\vec{v}^{\mathrm{T}}) - \frac{2}{3}\nabla.\vec{v}I\right] \quad (4.13)$$

where μ = molecular viscosity

I = unit tensor,

Within the framework of 2D axisymmetric geometries, the equations governing the conservation of axial and radial momentum can be articulated as follows:

$$\frac{\partial}{\partial x}(\rho v_x) + \frac{1}{r}\frac{\partial}{\partial x}(r\rho v_x v_x) + \frac{1}{r}\frac{\partial}{\partial r}(r\rho v_r v_r) = -\frac{\partial p}{\partial x} + \frac{1}{r}\frac{\partial}{\partial x}\left[r\mu\left(2\frac{\partial v_x}{\partial x} - \frac{2}{3}(\nabla.\vec{v})\right)\right] + \frac{1}{r}\frac{\partial}{\partial r}\left[r\mu\left(\frac{\partial v_x}{\partial r} + \frac{\partial v_r}{\partial x}\right)\right] + F_x \quad (4.14)$$

And

$$\frac{\partial}{\partial t}(\rho v_r) + \frac{1}{r}\frac{\partial}{\partial x}(r\rho v_x v_r) + \frac{1}{r}\frac{\partial}{\partial r}(r\rho v_r v_r) = -\frac{\partial p}{\partial r} + \frac{1}{r}\frac{\partial}{\partial x}\left[r\mu\left(\frac{\partial v_r}{\partial x} + \frac{\partial v_x}{\partial r}\right)\right] + \frac{1}{r}\frac{\partial}{\partial r}\left[r\mu\left(2\frac{\partial v_r}{\partial r} - \frac{2}{3}(\nabla.\vec{v})\right)\right] - 2\mu\frac{v_r}{r^2} + \frac{2\mu}{3r}(\nabla.\vec{v}) + \rho\frac{v_z^2}{r} + F_r \quad (4.15)$$

Where

$$\nabla.\vec{v} = \frac{\partial v_x}{\partial x} + \frac{\partial v_r}{\partial r} + \frac{v_r}{r} \quad (4.16)$$

Where v_x= Axial velocity

v_r= Radial velocity

A. $\boldsymbol{v_z}$ *= swirl velocity*

4.5.3 Energy Equation

The energy equation for the mixture is expressed as follows:

$$\frac{\partial}{\partial t}\sum_{k=1}^{n}(\alpha_k\rho_k E_k) + \nabla.\sum_{k=1}^{n}\left(\alpha_k\vec{v}_k(\rho_k E_k + p)\right) = \nabla.\left(k_{eff}\nabla T\right) + S_E \quad (4.17)$$

Where k_{eff} = effective conductivity

S_E= volumetric heat sources

$$E_k = h_k - \frac{p}{\rho k} + \frac{v_k^2}{2} \quad (4.18)$$

Where

$E_k = h_k$ for an incompressible phase and h_k= sensible enthalpy for phase *k*

$k-\in$ *model*

The turbulence kinetic energy, denoted as "k" and its dissipation rate, represented as "$\in$" are determined using the following transport equations:

$$\frac{\partial}{\partial t}(\rho k) + \frac{\partial}{\partial x_i}(\rho k v_i) = \frac{\partial}{\partial x_j}\left[\left(\mu + \frac{\mu_t}{\sigma_k}\right)\frac{\partial k}{\partial x_j}\right] + G_k + G_b - \rho \in -Y_M + S_k \quad (4.19)$$

and

$$\frac{\partial}{\partial t}(\rho \in) + \frac{\partial}{\partial x_i}(\rho \in v_i) = \frac{\partial}{\partial x_j}\left[\left(\mu + \frac{\mu_t}{\sigma_\in}\right)\frac{\partial \in}{\partial x_j}\right] + C_{1\in}\frac{\in}{k}(G_k + C_{3\in}G_b) - C_{2\in}\rho\frac{\in^2}{k} + S_\in \quad (4.20)$$

Within these equations, G_k denotes the generation of turbulence kinetic energy resulting from the mean velocity gradients.

S_k And $S_\in$ represents the user-defined source terms.

Y_M Represents the contribution of the fluctuating dilatation in compressible turbulence to the overall dissipation rate,

σ_k and $\sigma_\in$ are turbulent Prandtl numbers for k and$\in$,

$C_{1\in}$, $C_{2\in}$, and $C_{3\in}$ are constant.

G_b is the generation of turbulence kinetic energy due to buoyancy,

The Volume of fluid (VOF) model:

In situations where it is essential to simulate multiple unmixed liquids by solving a sequence of motion equations while monitoring the volume fraction of each fluid across the entire domain, we utilize the Volume-of-Fluid (VOF) method. Common applications of this approach encompass predictive modeling of reactive fission, the behavior of large bubbles within a liquid medium, and the motion of a liquid following the rupture of a barrier, "at any static or transient interface of the liquefied gas".

Volume Fraction Equation α_q

Characterizing multiphase flow as an intermediate continuum involves introducing the notion of phase-volume fractions, which we'll denote as α_q in this context. These volume fractions depict the spatial distribution of individual phases, allowing us to uphold the principles of mass and momentum conservation for each phase independently. The development of conservation equations within this framework is accomplished by the application of mixture theory.

The phase magnitude$q$,V_q is given by

$$V_q = \int_{v=1}^{n} \alpha_q dV \quad (4.21)$$

Where

$$\sum_{q=1}^{n} \alpha_{q=1} \quad (4.22)$$

The effective density of phase q is

$\hat{\rho}_q = \alpha_q . \rho_q$

Where ρ_q is the physical density of phase$q$.

E. CAD modeling of single slope solar still

The generation of a three-dimensional CAD model for a single-slope solar still was accomplished through the utilization of ANSYS Design Modular. This software played a pivotal role in the modeling process, providing a robust platform for the creation of a detailed and accurate representation of the solar still's geometry. The application of ANSYS Design Modular ensured a comprehensive and efficient approach to constructing the CAD model, facilitating a thorough representation of the intricate design elements and geometric features inherent in the single-slope solar still. This modeling endeavor serves as a foundational step in the comprehensive analysis and simulation of the solar still system. The model was designed with precise dimensional specifications, featuring a base measuring 1.1 meters by 1.1 meters. The front wall was set to a height of 0.25 meters, while the back wall extended to a height of 0.9 meters. A graphical representation of this 3D CAD model of the solar still can be observed in the provided.

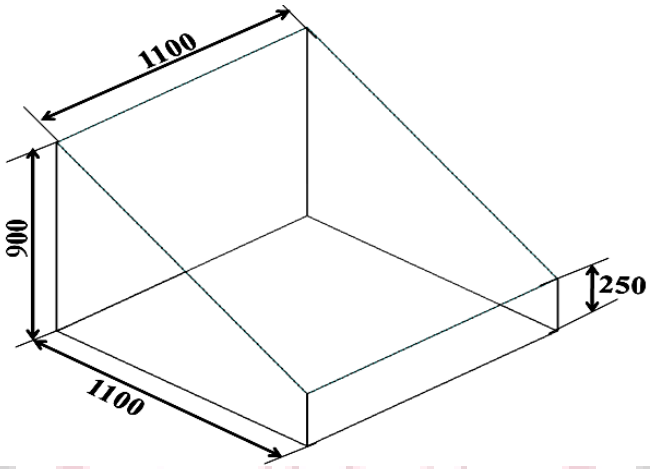

Fig. 5 3D CAD model of the solar still

Meshing: the pivotal step in the finite element analysis comes after the CAD geometry of the single slope solar system has been imported into ANSYS Workbench for subsequent analysis. During this phase, the CAD geometry is divided into many smaller units referred to as a "mesh". The mesh generation process for the simple slope solar panel in this study is shown in Figure [insert figure number]. The total number of nodes is 137,076, while the total number of elements is 128,643, all consisting of hexahedral type elements.

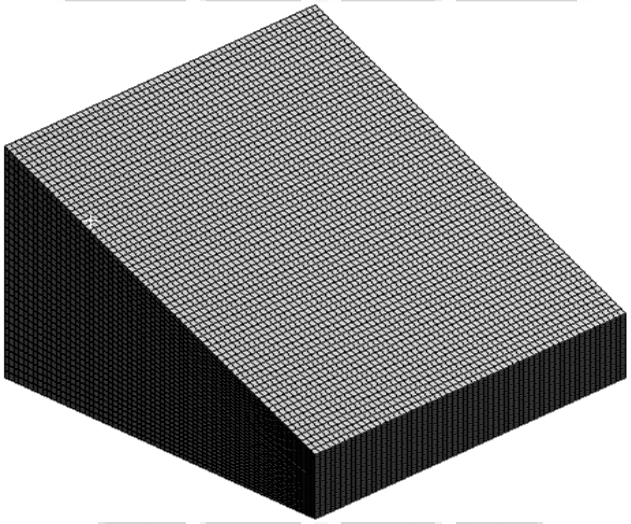

Fig. 6 Meshing

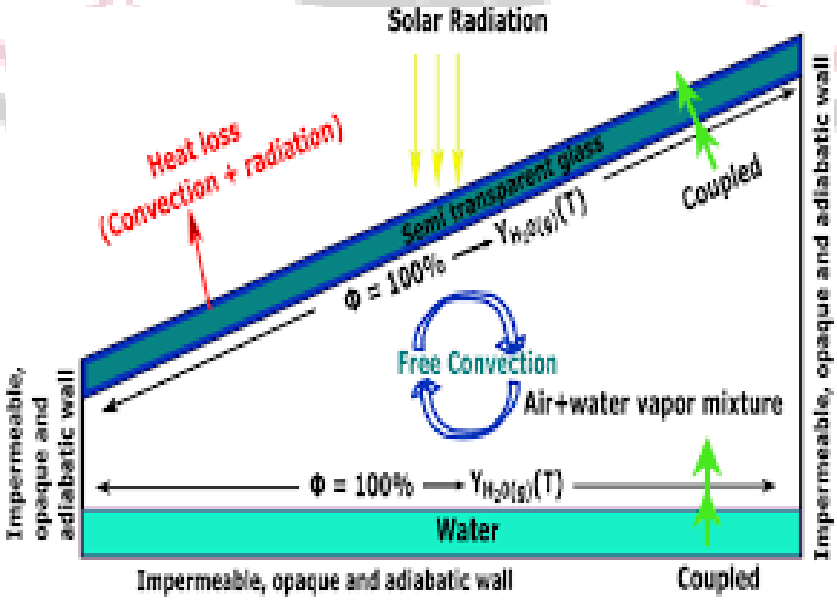

Fig. 7 Heat Transfer in Solar Distillation

Material properties:

Table 4.1: Paraffin C18 material's thermo physical property

Properties	Values measured
Heating state	
Solid–solid phase change temperature	Tpm=5.08∘C
Melting point	Tm=25.53∘C−25.69∘C
Latent heat of solid-solid change	Lpm=23.692J/g
Latent heat of melting	Lm=155.960J/g−140.581J/g
Cooling state	
Solid-solid phase change temperature	Tpc=3.95∘C
Crystallization point	Tc=26.2∘C
Latent heat of solid-solid change	Lpc=22.594J/g
Latent heat of crystallization	Lc=162.165J/g−154.848J/g
Specific heat of solid	Cps(≤15∘C)=3.25±0.35J/g·∘C
Specific heat of liquid	Cpl(≥40∘C)=2.23±0.005J/g·∘C

4.7 Boundary conditions

- For fluid flow due to natural convection, set the gravitational acceleration in the –y direction to 9.81 m/s2.
- Use a multiphase model as an implicit VOF (Volume of fluid) formulation using an Eulerian phase number of 03 (air, water-liquid, and water vapor).
- Demand on the energy equation, even when heat transfer occurs.
- In the viscous model, select k-epsilon with the standard wall function turbulence model
- Solar radiation was directed onto the glass cover of the solar still, positioned at a global coordinate of 76.8 longitude, 23.2650 latitude, and within a +5.5-hour time zone to ensure optimal weather conditions.
- In a multiphase evaporation-condensation interaction for the steam-to-steam and steam-to-water mass transfer mechanism.
- Choose Second Order Upwind for the momentum and energy equation.
- A smooth solver is used to solve this CFD problem.

F. Validation of the work

The primary objective of this study is to determine the maximum achievable water output from a double slope solar still and then assess and compare their respective efficiencies. To validate our research, we referred to a scholarly work from 2020 authored by C. Gnanavel et al., titled "CFD Analysis of a Solar Device with PCM," which was published in Materials Today: Proceedings. This source is available online through Science Direct with the following DOI: doi.org/10.1016/j.matpr.2020.05.638. Our research predominantly involved computational fluid dynamics (CFD) analysis, wherein we created three-dimensional CAD models for both single and double-slope solar stills. The models were meticulously designed using ANSYS Design Modular software, adhering to specific dimensions that included a 1.1m x 1.1m base, a 0.25m front wall, and a 0.9m back wall. By drawing upon this established study and employing advanced modeling techniques, we aimed to enhance the credibility and robustness of our research methodology in examining the thermal dynamics of solar still configurations. The results obtained from our analysis were then compared with the findings reported in the reference.

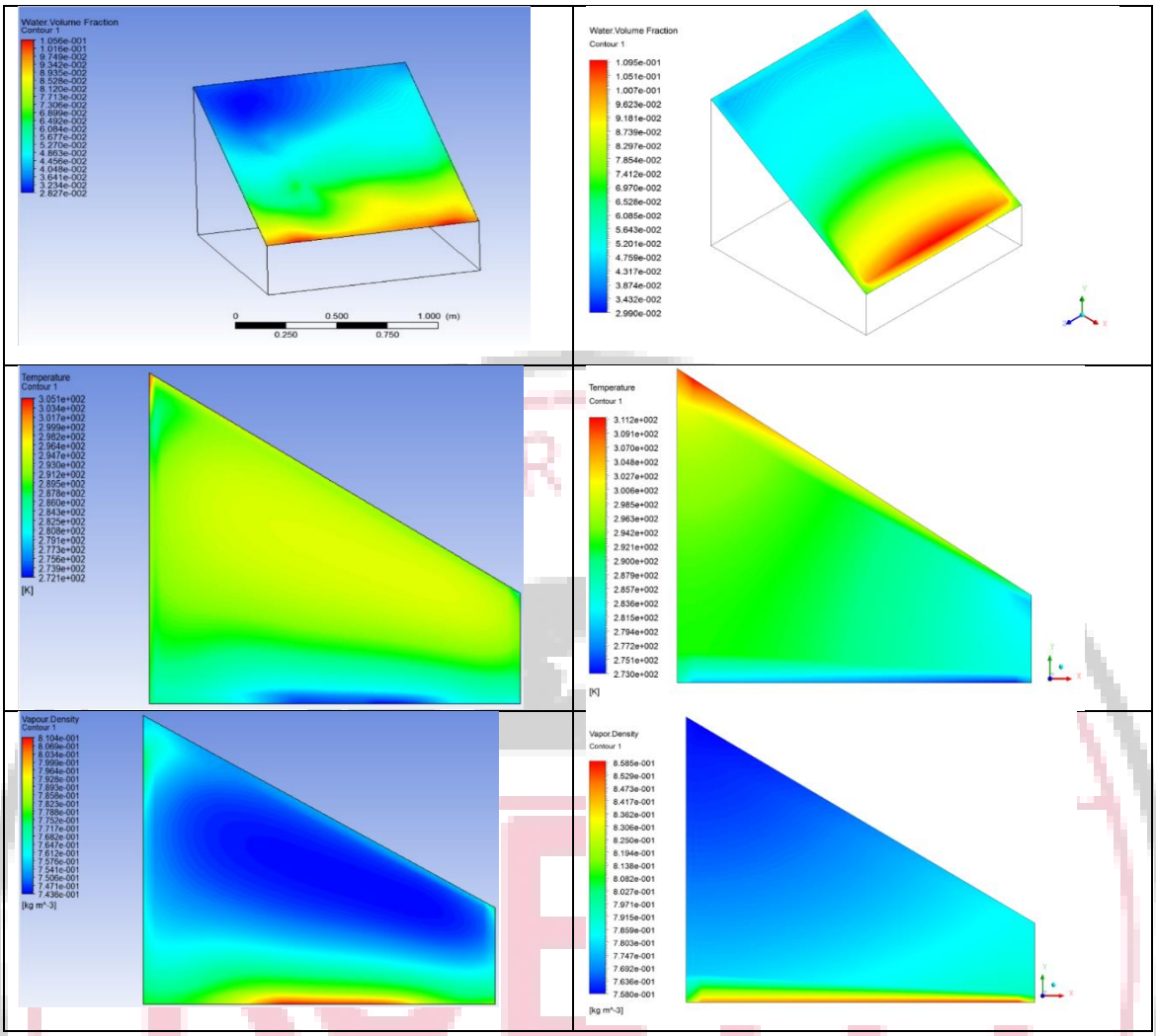

Fig. 8 Validation of work water volume fraction, Temperature, Vapour density

From the above contours diagram it has been observed that Volume fraction of water showing 3.69% variation while the temperature difference of 6.1 degree showing 1.99% variation and the vapour density showing 5.94% variation. All above compared results show very good agreement between base paper and present work, hence the further analysis with same boundary with modified design have to be done.

Table 4.2 Comparing parameters with C. Gnanavel et al.'s 2020 study and our present work

S. No	**Parameters**	Volume fraction of water	Temperature (K)	Vapor density (Kg/m^3)
1	**C. Gnanavel et al 2020**	0.1042	0.1095	3.69%
2	**Present work**	303.1	311.2	1.99%
3	**% Difference**	0.7104	0.8585	5.94 %

V. RESULT AND DISCUSSION

The central focus of this research is to evaluate the maximum water output achievable from a double-slope solar still basin and conduct a comparative productivity analysis with a single-slope solar still. To achieve this goal, advanced three-dimensional computer-aided design (CAD) models were developed for both single and double-slope solar stills. Computational fluid dynamics (CFD) analysis was then performed using the ANSYS design module to delve into the thermal and fluid dynamics within the solar still configurations. This integrated approach enables a comprehensive assessment of the water production potential of double-slope solar stills while facilitating a meaningful comparison with single-slope counterparts. The study aims to provide valuable insights into the efficiency and performance of different solar

still designs, contributing to the optimization of freshwater production methods. Using VOF implicit formulation, the analysis utilized a multiphase model that took into consideration the phases of air, water-liquid, and water-vapor, as well as the incorporation of evaporation-condensation for mass transfer mechanisms. Paraffin C18 was used as the nanofluid in the solar stills, which were subjected to sun radiation under particular meteorological conditions. This chapter presents the findings and contours derived from the computational fluid dynamics study.

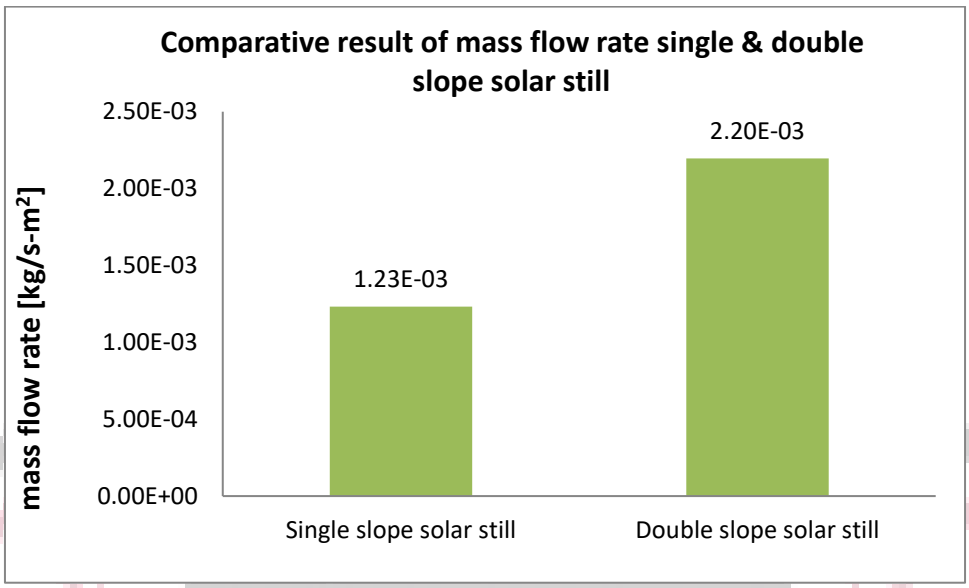

Fig. 9 Comparative result of mass flow rate single & double slope solar still

After comparing the mass flow rates of single and double slope solar stills, the results show that the double slope solar still has a mass flow rate that is 0.00097 times higher than the single slope solar still.

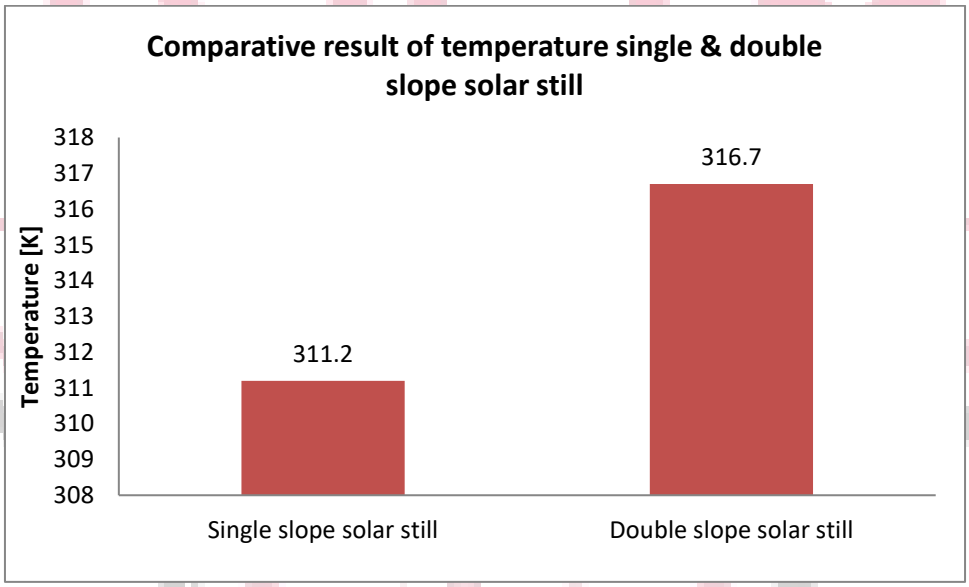

Fig. 10 Comparative result of temperature single & double slope solar still

Following a thorough comparative evaluation of the fluid temperature distribution between the two distinct types of solar stills, it became evident that in the case of the double-slope solar still, there was an increase of 5.5 degrees. This marked a 1.77% higher temperature compared to the single-slope solar still. The observed temperature variations provide valuable insights into the thermal performance discrepancies between these two solar still configurations, offering essential information for further analysis and potential enhancements in their design and functionality.

A. Productivity of single slop solar still

This equation is used to calculate the hourly productivity

$$P_h = \frac{h_{evap}\,(T_w - T_g)\times 3600}{\lambda} \qquad (5.1)$$

Table: 5.2: Latent heat of vaporization of water

Temperature [°C]	**Latent heat of vaporization of water λ [kJ/kg]**	**Temperature [°C]**	**Latent heat of vaporization of water λ [kJ/kg]**
0.01	2500.90	96.00	2266.90
2.00	2496.20	100.00	2256.40
4.00	2491.40	110.00	2229.60
10.00	2477.20	120.00	2202.10
14.00	2467.70	140.00	2144.30
18.00	2458.30	160.00	2082.00
20.00	2453.50	180.00	2014.20
25.00	2441.70	200.00	1939.70
30.00	2429.80	220.00	1857.40
34.00	2420.30	240.00	1765.40
40.00	2406.00	260.00	1661.60
44.00	2396.40	280.00	1543.00
50.00	2381.90	300.00	1404.60
54.00	2372.30	320.00	1238.40
60.00	2357.70	340.00	1027.30
70.00	2333.00	360.00	719.80
80.00	2308.00	373.95	0.00
90.00	2282.50	*https://www.engineeringtoolbox.com/water-properties-d_1573.html*	

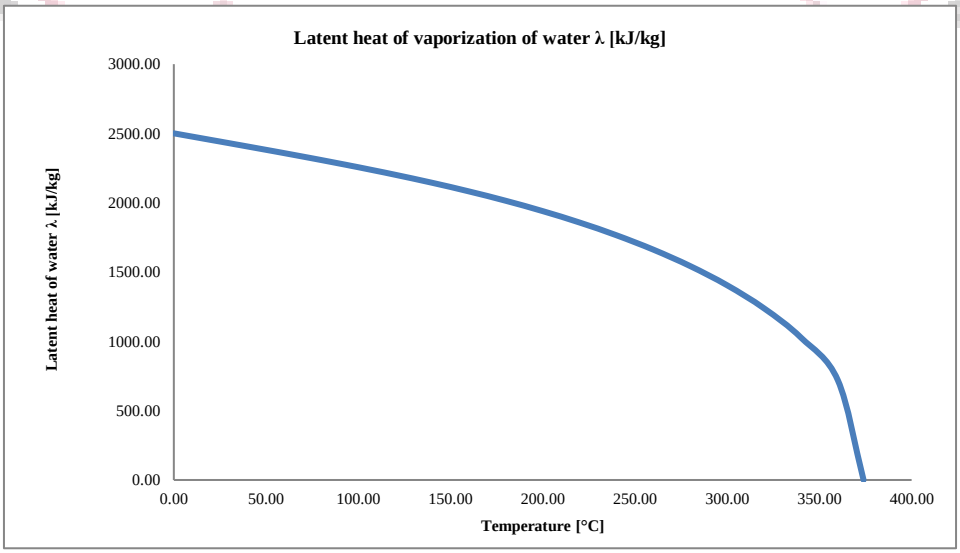

Fig. 11 Latent heat of vaporization of water λ [kJ/kg]

h_{evap} = Evaporation heat transfer coefficient between the basin water and the glass

$$h_{evap} = 16.273 \times 10^{-3} \times h_c \times \left[\frac{P_w - P_g}{T_w - T_g}\right] \quad (5.2)$$

h_c = Convective heat transfer coefficient from basin water to glass cover

P_w = Vapour pressure of basin water

P_g= Vapour pressure of glass water

$$P = \exp\left[25.317 - \frac{5144}{T+273}\right]$$

T_w= Temperature of water (38.2 ºC) obtained from CFD simulation

$$T_g = \frac{T_{in}+T_{out}}{2} \quad (5.3)$$

Let T_{in}= 25 ºC

$T_w = T_{out}$ = 38.2 ºC

$T_g = \frac{25+38.2}{2} = 31.6$ ℃

$$P_w = \exp\left[25.317 - \frac{5144}{T_w+273}\right]$$

$$P_w = \exp\left[25.317 - \frac{5144}{38.2+273}\right]$$

$$\boldsymbol{P_w = 6551.42\ Pa}$$

$$P_g = \exp\left[25.317 - \frac{5144}{T_g+273}\right]$$

$$P_g = \exp\left[25.317 - \frac{5144}{31.6+273}\right]$$

$$\boldsymbol{P_g = 4579.195\ Pa}$$

$$h_c = 0.884\left[T_w - T_g + \left\{\frac{(P_w - P_g)(T_w+273)}{268900 - P_w}\right\}\right]^{1/3}$$

$$h_c = 0.884\left[38.2 - 31.6 + \left\{\frac{(6551.42 - 4579.195)(38.2+273)}{268900 - 6551.42}\right\}\right]^{1/3}$$

$$\boldsymbol{h_c = 7.008\ {}^{W}/_{m^2.k}}$$

$$h_{evap} = 16.273 \times 10^{-3} \times 7.008 \times \left[\frac{6551.42 - 4579.195}{38.2 - 31.6}\right]$$

$$\boldsymbol{h_{evap} = 34.078\ {}^{W}/_{m^2.k}}$$

λ = Latent heat of vaporization of water during the day 2410.29 [kJ/kg]

$$P_h = \frac{h_{evap}\,(T_w - T_g) \times 3600}{\lambda} \quad (5.4)$$

$$P_h = \frac{34.078\,(38.2 - 31.6) \times 3600}{2410.29}$$

$$\boldsymbol{P_h = 335.93\ ml/hr}$$

The daily productivityP_d given by

$$P_d = \sum_{24\ hr} P_h$$

$$P_d = \sum_{24\ hr} 335.93$$

$$\boldsymbol{P_d = 8398.25\ ml/day}$$

Productivity of double slop solar still

T_w= Temperature of water (43.7 ºC) obtained from CFD simulation

$T_g = \frac{25+43.7}{2} = 34.35$ ℃

$$P_w = \exp\left[25.317 - \frac{5144}{43.7+273}\right]$$

$$\boldsymbol{P_w = 8729.813\ Pa}$$

$$P_g = \exp\left[25.317 - \frac{5144}{34.35+273}\right]$$

$$\boldsymbol{P_g = 5326.132\ Pa}$$

$$h_c = 0.884\left[43.7 - 34.35 + \left\{\frac{(8729.813 - 5326.132)(43.7+273)}{268900 - 8729.813}\right\}\right]^{1/3}$$

$$\boldsymbol{h_c = 9.685\ {}^{W}/_{m^2.k}}$$

$$h_{evap} = 16.273 \times 10^{-3} \times 9.685 \times \left[\frac{8729.813 - 5326.132}{43.7 - 34.35}\right]$$

$$\boldsymbol{h_{evap} = 57.37\ {}^{W}/_{m^2.k}}$$

λ = Latent heat of vaporization of water during the day 2397.12 [kJ/kg]

$$P_h = \frac{h_{evap}\,(T_w - T_g) \times 3600}{\lambda} \tag{5.5}$$

$$P_h = \frac{57.37(43.7 - 34.35) \times 3600}{2397.12}$$

$$\boldsymbol{P_h = 805.58\ ml/hr}$$

The daily productivity P_d given by

$$P_d = \sum_{24\ hr} P_h$$

$$P_d = \sum_{24\ hr} 805.58$$

$$\boldsymbol{P_d = 20139.5\ ml/day}$$

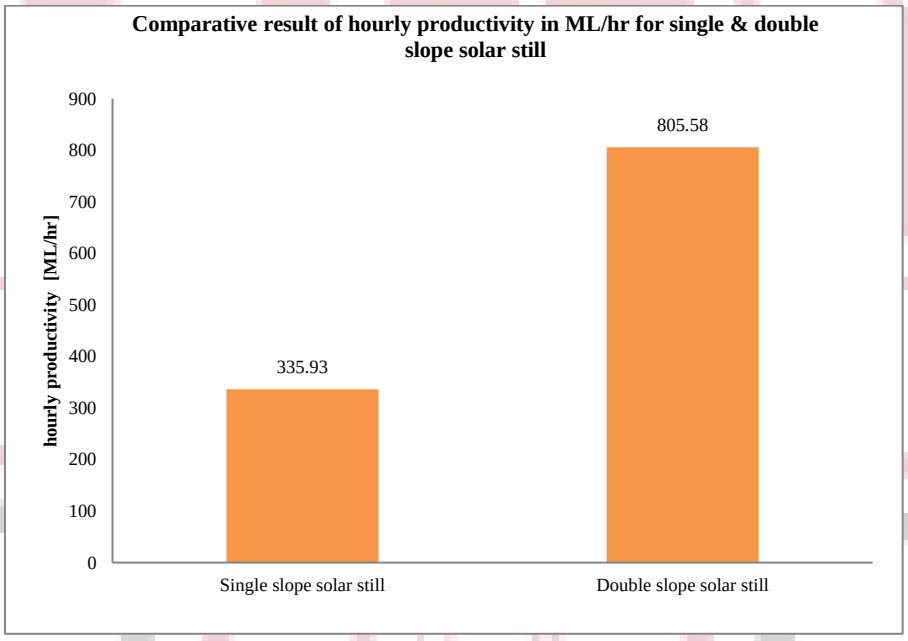

Fig. 12 Comparative result of hourly productivity in ML/hr for single & double slope solar still

By comparing the hourly output of the double-slope and single-slope solar stills, it becomes evident that the double slope solar still outperforms the single slope solar still with a 1.398 times higher hourly productivity.

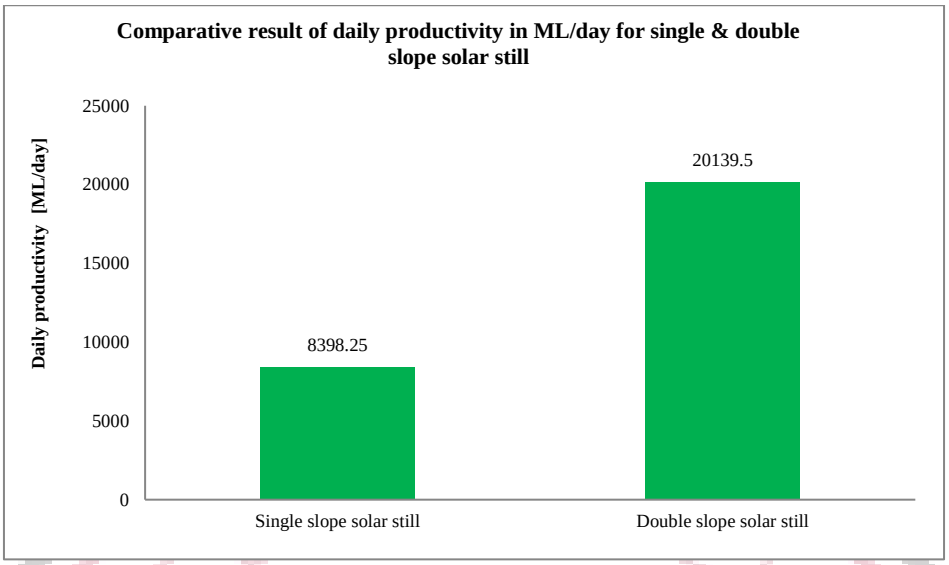

Fig. 13 Comparative result of daily productivity in ML/day for single & double slope solar still

Upon evaluating the daily productivity of the two solar systems, it is evident that the double-slope solar still outperforms the single-slope solar still, yielding a higher output by a factor of 1.398. Additionally, when comparing the results with a single-slope solar still, the analysis indicates that a temperature increase of 5.5 degrees Kelvin corresponds to a remarkable 1.398-fold increase in daily productivity. These findings underscore the substantial impact of temperature variations on the overall efficiency and productivity of solar still systems, particularly highlighting the advantageous performance of the double-slope configuration.

V. CONCLUSION

The research conducted in this study offers significant insights into the advancements of solar-powered distillation systems. The comparative analysis between single-slope and double-slope solar stills using CFD and CAD models revealed a notable increase in water output and efficiency in the double-slope configuration. This superiority is attributed to the more effective capture of solar energy and enhanced thermal performance, leading to higher evaporation rates. The findings emphasize the potential of double-slope solar stills in addressing the growing demand for freshwater, particularly in arid regions. The study underscores the importance of continuous innovation in solar distillation technologies, suggesting that further optimization in design and materials could yield even greater efficiency gains. This advancement in distillation technology not only contributes to sustainable freshwater production but also represents a significant step towards addressing global water scarcity challenges.

REFERENCES

[1] Siliang Chen et. al. "A floating solar still inspired by continuous root water intake" Desalination 512 (2021) 115133. https://doi.org/10.1016/j.desal.2021.115133.

[2] D.E. Benhadji Serradj et al. "The use of passive baffles to increase the yield of a single slope solar still" Solar Energy 226 (2021) 297–308. https://doi.org/10.1016/j.solener.2021.08.054.

[3] Md Hemmat Esfe et al. "Optimization of influential geometrical parameters of single slope solar still equipped with thermoelectric system to achieve maximum desalinated water" Energy Reports 7 (2021) 5257–5268. https://doi.org/10.1016/j.egyr.2021.08.106.

[4] Md Hemmat Esfe et al. "Simulation of the impact of solar radiation intensity on the performance of economical solar water desalination still in Semnan province" Case Studies in Thermal Engineering 28 (2021) 101471. https://doi.org/10.1016/j.csite.2021.101471.

[5] Shahin Shoeibi et al. "A comprehensive review of Enviro-Exergo-economic analysis of solar stills" Renewable and Sustainable Energy Reviews 149 (2021) 111404. https://doi.org/10.1016/j.rser.2021.111404.

[6] Shahin Shoeibi et al. "Energy matrices, exergoeconomic and enviroeconomic analysis of aircooled and water-cooled solar still: Experimental investigation and numerical simulation" Renewable Energy 171 (2021) 227e244. https://doi.org/10.1016/j.renene.2021.02.081.

[7] Sivakumar, V., & Sundaram, E. G. (2013). Improvement techniques of solar still efficiency: A review. *Renewable and Sustainable Energy Reviews*, *28*, 246-264. https://doi.org/10.1016/j.rser.2013.07.037

[8] Samee, M. A., Mirza, U. K., Majeed, T., & Ahmad, N. (2017). Design and performance of a simple single basin solar still. *Renewable and Sustainable Energy Reviews*, *11*(3), 543-549.https://doi.org/10.1016/j.rser.2005.03.003

[9] Kabeel, A. E., & El-Agouz, S. A. (2011). Review of researches and developments on solar stills. *Desalination*, *276*(1-3), 1-12. https://doi.org/10.1016/j.desal.2011.03.042

[10] Nayi, K. H., & Modi, K. V. (2018). Pyramid solar still: a comprehensive review. *Renewable and sustainable energy reviews*, *81*, 136-148. https://doi.org/10.1016/j.rser.2017.07.004

[11] Sathyamurthy, R., El-Agouz, S. A., Nagarajan, P. K., Subramani, J., Arunkumar, T., Mageshbabu, D., ... & Prakash, N. (2017). A review of integrating solar collectors to solar still. *Renewable and Sustainable Energy Reviews*, *77*, 1069-1097.https://doi.org/10.1016/j.rser.2016.11.223

[12] Panchal, H. N., & Patel, S. (2017). An extensive review on different design and climatic parameters to increase distillate output of solar still. *Renewable and Sustainable energy reviews*, *69*, 750-758.https://doi.org/10.1016/j.rser.2016.09.001

[13] Kadhum, J. A. (2018). Exploitation of solar energy in the process of purification of the land surface water. *International Journal of Computation and Applied Sciences IJOCAAS*, *5*(1), 356-360.